



Cite this: *RSC Adv.*, 2023, **13**, 28250

## A novel method for synthesis of carbon dots and their applications in reactive oxygen species (ROS) and glucose detections

Chao-Sheng Chen,<sup>a</sup> Aaron Shinnosuke Yokokawa,<sup>b</sup> Kuan-Hsun Tseng,<sup>c</sup> Ming-Hsu Wang,<sup>d</sup> Kevin Sheng-Kai Ma<sup>ef</sup> and Chin-Feng Wan<sup>ID \*g</sup>

A simple and novel method is proposed for preparation of water-soluble fluorescent carbon dots (C-dots), which have potential to be applied in detecting reactive oxygen species (ROS). The C-dots with high fluorescence quantum yield were created by hydrothermal methods with lactose as the carbon source and tris(hydroxymethyl)aminomethane (Tris) as the surface passivation reagent. The C-dots have some unique characteristics such as excellent biocompatibility with a broad pH working range of 5–11 and high fluorescence, which makes them especially useful in the bio-detection field. The optical properties, surface groups, and element components of the prepared C-dots have been systematically studied by fluorescence spectroscopy. This facile approach is efficient and environmentally friendly and allows large-scale production of the C-dots without any further post-treatment. The C-dots have been adopted as probes for fluorescence turn-off detection owing to their high sensitivity to the hydroxyl radical. The detection limit can reach  $\sim 0.1 \mu\text{M}$  under optimized conditions when using hydrogen peroxide as the source for generating ROS. Moreover, when paired with glucose oxidase, these C-dots can track glucose concentrations in samples. This adaptability suggests their potential in detecting various metabolites, paving the way for practical uses in disease detection.

Received 18th March 2023

Accepted 11th September 2023

DOI: 10.1039/d3ra01795h

rsc.li/rsc-advances

## 1. Introduction

### 1.1 Carbon dots

Carbon dots (C-dots), a new type of fluorescent carbon nanoparticle, have garnered considerable attention since they were first reported in 2004 by Xu *et al.*<sup>1</sup> who were purifying single-walled carbon nanotubes. In the last few years, C-dots have been explored because of their facile synthesis, easy surface modification, favorable optical properties, high biocompatibility, outstanding water solubility, low toxicity, and eco-friendly nature. These properties make C-dots a better candidate than the well-known semiconductor quantum dots for various applications,<sup>2–9</sup> including small-molecule sensing, photocatalytic reactions, and biological applications such as

biomolecular sensing, cellular imaging, photothermal therapy, and photodynamic therapy. Moreover, the facile and low-cost synthesis of C-dots offers a unique advantage in nanotechnology in terms of rapid and cost-effective production.

Multiple methods have been developed for creating customized C-dots with specific properties suited for various applications. Broadly speaking, these widely recognized synthesis approaches for C-dots can be categorized as either “top-down” or “bottom-up” strategies.<sup>10</sup> Unlike top-down synthesis methods, bottom-up approaches employing carefully controlled synthetic conditions with small organic precursors enable the creation of more homogeneous C-dots and allow a diverse range of functional groups on their surface. The precursors initiate chemical transformations, fragmentation, and self-assembly processes under high-temperature and high-pressure conditions, leading to the formation of small carbonaceous structures. The carbon-rich intermediates undergo further reactions that result in the formation of small carbon clusters or nanoparticles. These clusters can be stabilized and passivated by the reaction with functional groups present in the reaction mixture. Surface passivation agents, such as organic molecules or polymers, may also be present in the reaction mixture. These passivating agents can adsorb onto the growing carbon dots’ surface, stabilizing the structure and preventing further uncontrolled growth.<sup>10,11</sup>

<sup>a</sup>Department of Life Science, Imperial College London, London, UK

<sup>b</sup>Department of Electrical Engineering, National Sun Yat-sen University, Kaohsiung, Taiwan

<sup>c</sup>Department of Life Science, National Taiwan Normal University, Taipei, Taiwan

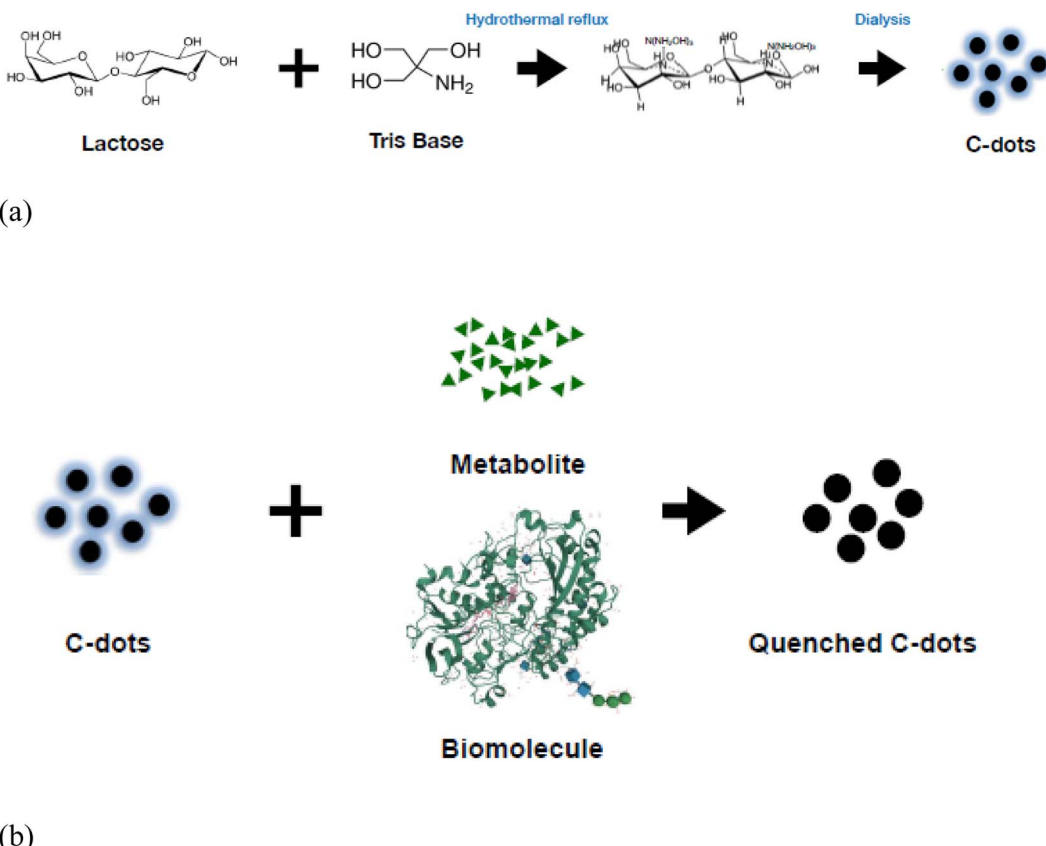
<sup>d</sup>Center for General Education, Affiliated with College of Interdisciplinary Studies, Taipei Medical University, Taipei, Taiwan

<sup>e</sup>Graduate Institute of Biomedical Electronics and Bioinformatics, National Taiwan University, Taipei, Taiwan

<sup>f</sup>Department of Dentistry, Chung Shan Medical University and Hospital, Taichung, Taiwan

<sup>g</sup>Department of Medical Applied Chemistry, Chung Shan Medical University, Taichung, Taiwan. E-mail: jeanwan04@gmail.com





Scheme 1 (a) Green synthesis of carbon dots. (b) Mechanisms underlying the reaction between metabolite, biomolecule and the C-dots.

## 1.2 Reactive oxygen species

Reactive oxygen species (ROS) are naturally produced during the typical oxygen metabolism and play roles in various physiological processes and diseases.<sup>12–14</sup> Although ROS can be harmful when they are abundant, they are key signaling molecules. Therefore, the maintenance of suitable ROS levels is crucial to the integrity and survival of living organisms. Aberrant levels of ROS are associated with various pathological processes. For instance, the currently aggressive use of antibiotics, antivirals, and chemotherapeutic drugs may cause unwanted tissue inflammation and organ (*e.g.*, liver and kidney) injury, thus increasing the *in vivo* levels of ROS and resulting in an additional stress burden. Therefore, real-time and deep-tissue imaging techniques are urgently needed for monitoring the *in vivo* levels of ROS; such monitoring is important for exploring various biological processes, treating several diseases, and evaluating drug toxicities. Furthermore, because of the distinct sources and biological effects of ROS, differential visualization of ROS may offer additional insights that could shed light on how ROS impact on relevant biological processes.<sup>12–14</sup> Considerable effort has been invested in this field. Several imaging probes have been developed that can detect various types of ROS (*e.g.*,  $O_2^-$ ,  $H_2O_2$ ,  $OH^-$ ,  $O_3$  etc.). And these probes offer potential solutions for the *in vivo* detection of ROS.<sup>15–17</sup> Most of these probes contain fluorescent dyes or nanoparticles.

In this study, we introduce a straightforward hydrothermal technique to produce highly fluorescent C-dots using a mixture of

lactose and Tris. These C-dots serve as effective probes for fluorescence turn-off detection due to their sensitivity to the hydroxyl radical. Notably, the fluorescence intensity of these C-dots diminishes in the presence of the hydroxyl radical, allowing for the real-time tracking of glucose levels when the C-dots are coupled with glucose oxidase (as depicted in Scheme 1). The C-dots sensor can distinctly identify glucose even when mixed with up to three other saccharides, all without the need for prior sample preparation. We anticipate these C-dots to be versatile tools for broad metabolite monitoring. Their low toxicity also suggests potential applications in diverse detection methodologies.

## 2. Materials and methods

### 2.1 Reagents and chemicals

Lactose,  $Na_2HPO_4$ ,  $NaH_2PO_4$ , potassium phosphate, Tris-HCl, and  $NaHCO_3$  were purchased from Sigma-Aldrich.  $\beta$ -Glucose oxidase was obtained from Sigma-Aldrich. Dialysis membrane pre-treated RC tubing MWCO: 1 kDa (vol/length: 4.6  $mL\ cm^{-1}$ ) was purchased from Spectrum Laboratories, Inc., Rancho Dominguez, CA, USA. Luminescent C-dots were synthesized in our laboratory. All reagents were of analytical grade or higher and used as received without further treatment.

### 2.2 Instrumentation

All fluorescence experiments were performed using the Hitachi 2500 spectrometer. Ultraviolet-visible (UV-vis) spectroscopic



analyses were performed using the SPECTROstar Nano (BMG LABTECH, Germany). High performance liquid chromatography (HPLC) experiments were performed using the Shimadzu, SPD-20, LC-20AT, C-18 column.

### 2.3 Synthesis and purification of luminescent C-dots

Luminescent C-dots were synthesized *via* a single-step hydrothermal pathway (Scheme 1). In brief, 0.125 g of lactose and 2.0 g of Tris were dissolved in 40 mL pure water in a round bottom flask. The pH of the mixture was 10.5. It was hydrothermally refluxed at 100 °C with stirring for 8 hours until the colorless solution turned yellow. The boiling-hot C-dot solution was maintained at 25 °C for 3 days until the lactose had reacted completely with Tris. The pH was neutralized with HCl and dialyzed against pure water. The purification phase extended over 11 hours, utilizing a dialysis membrane pre-treated RC tubing with a 65 mL capacity (with MWCO 1 kDa). To ensure the comprehensive purification of the C-dots, a combination of fluorescence spectroscopy and HPLC chromatography systems tracked the process at intervals: 0 hours, 7 hours, 10 hours, and 11 hours into the dialysis.

### 2.4 Analysis and characterization of C-dots

The synthesized C-dots were subjected to further analysis by TEM, FT-IR, XPS and XRD. X-ray diffraction (XRD) patterns were measured on a D2 diffractometer (Bruker-D2 Phaser, Germany) using Cu K $\alpha$  radiation (30 kV, 10 mA, and 2 theta). The molecular structures of the C-dots synthesized were detected by a FT-IR spectrometer (Bruker Optics FT-IR, Alpha OPUS, Germany). The spectra (over the range 600–4000  $\text{cm}^{-1}$ ) were collected by scans with a resolution of 2  $\text{cm}^{-1}$ . The Escalab 250 X-ray photoelectron spectrometer (XPS) (ULVAC PHI, Versa Probe 4 Japan) with a mono X-ray source Al K $\alpha$  excitation (0.5 eV, Ag 3d<sub>5/2</sub>) was used to characterize the content and the types of bonding of various elements in the samples. For morphological investigation, transmission electron microscope (TEM) images were provided which were obtained on a HT 7700 transmission electron microscope (HITACHI, Japan).

### 2.5 Stability of C-dots

To evaluate the stability of the synthesized C-dots, their response to changes in pH, ionic strength, and exposure duration was investigated. The C-dots solution was subjected to different pH levels (pH 5, 7, 9, and 11) by adjusting with hydrochloric acid (HCl) and sodium hydroxide (NaOH). Subsequently, the UV absorbance and fluorescence intensity of the C-dots sample were measured after a 10 minute interval. The impact of ionic strength on C-dots was further studied using potassium chloride (KCl). Various KCl solutions were prepared at concentrations of 0.2 M, 0.4 M, 0.6 M, 0.8 M, and 1.0 M. Subsequently, 5 mL of C-dots solution was added to each KCl solution in centrifugal tubes. The resulting mixtures were allowed to react for 10 minutes and subjected to UV-vis spectroscopy and photoluminescence spectrum measurements upon excitation at 348 nm.

To verify the photo stability of the C-dots, the C-dots solution was exposed to continuous UV radiation for a duration of 180 minutes to exam its photo stability. At intervals of 15 minutes,

1 mL of the solution was extracted to measure its UV absorption and photoluminescence intensity. This step was repeated throughout the entire 180 minute exposure period to monitor any changes in the UV absorption and photoluminescence properties of the C-dots over time.

### 2.6 Selectivity and interference measurements of C-dots

For the selectivity test, a mixture of 300  $\mu\text{L}$  glucose (0.1 M) and 25  $\mu\text{L}$  of glucose oxidase (0.1 g/5 mL) solution was added into a cuvette, allowing the enzyme reaction to proceed for roughly 30 minutes. Separate aliquots of different ion solutions, including uric acid, L-ascorbic acid,  $\text{Fe}^{3+}$ ,  $\text{Ca}^{2+}$ ,  $\text{Pb}^{2+}$ ,  $\text{Mg}^{2+}$ , and  $\text{K}^+$  (each at 100  $\mu\text{L}$  and  $1 \times 10^{-5}$  M), were each mixed with 300  $\mu\text{L}$  of the C-dots, and then combined with the pre-incubated enzyme reaction solution. The fluorescence intensity of individual mixtures was subsequently recorded. The interference of different ions on C-dot's  $\text{H}_2\text{O}_2$  detection was determined by comparing fluorescence intensities of individual C-dots/enzyme reaction mixture containing different ions.

### 2.7 Preparation and characterization of $\beta$ -glucose oxidase/C-dots biocomposite

The C-dots (2 mg  $\text{mL}^{-1}$ ) were subjected to sonication, centrifugation, and dialysis to remove small unreacted lactose particles and were then stirred for 30 min. Afterward, freshly prepared  $\beta$ -glucose oxidase solution (20 mg  $\text{mL}^{-1}$ ) was mixed with 0.1 M glucose for 30 min then added the C-dots solution and stirred for 1 min. The hybrid biocomposite was sonicated and centrifuged at 1500 rpm to remove aggregates. Samples of this mixture were carefully collected and analyzed using UV-vis spectroscopy and fluorescence spectroscopy to verify that the  $\beta$ -glucose oxidase had reacted completely with the C-dots. All experiments were performed at least triplicate to ensure reproducibility. Scheme 1 presents a schematic showing the mechanisms underlying the reaction between  $\beta$ -glucose oxidase and the C-dots.

### 2.8 $\beta$ -Glucose oxidase/C-dots biocomposite stability in pH buffers

The stability of the aforementioned biocomposite was evaluated at seven pHs: those of pH 5, 6, 7, 8, 9, 10, and 11. The aqueous pH was established at 0.05 M by using the following buffers:  $\text{Na}_2\text{HPO}_4 + \text{NaH}_2\text{PO}_4$  (pH 5.0),  $\text{Na}_2\text{HPO}_4 + \text{NaH}_2\text{PO}_4$  (pH 6.0), potassium phosphate (pH 7.0), HCl + Tris (pH 8.0 and 9.0), and  $\text{NaHCO}_3$  (pH 10.0 and 11.0); the ionic strength was adjusted to 0.20 M by using NaCl.

## 3. Results and discussion

### 3.1 Purification and characterization of the synthesized C-dots

The emergence of unwanted byproducts, residual precursors, or impurities is a common occurrence during the synthesis of C-dots. Therefore, it is necessary to further purify the reaction products *via* dialysis before further applications. The results for these C-dots, both from fluorescence spectrophotometer and HPLC, are depicted in Fig. 1 at intervals of 0 h, 7 h, 10 h, and



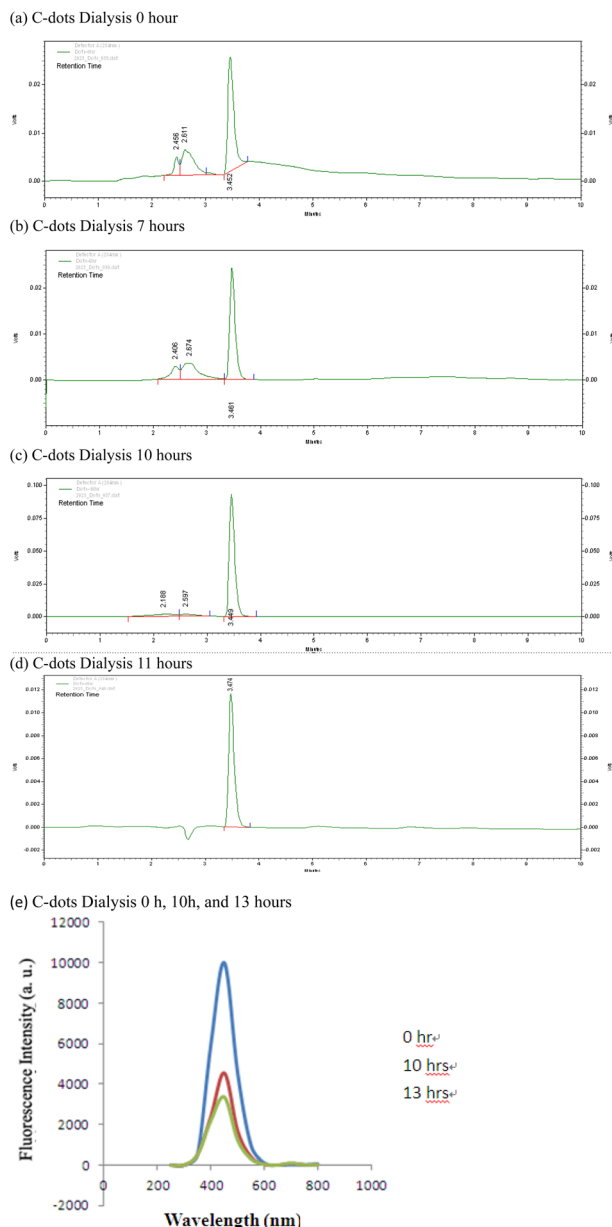


Fig. 1 HPLC chromatogram (a–d) and fluorescence spectrophotometer (e) of C-dots at different dialysis times.

11 h post-dialysis. Interestingly, Beatrice Bartolomei and Maurizio Prato<sup>18</sup> noted that C-dots derived from RR-Dphen, *o*-phenylenediamine (*o*-PDA) and L-Trp require approximately 120 h for complete purification, a duration surpassing the usual dialysis timeframes typically mentioned in C-dot studies. This finding suggests that many purification efforts might not be thorough enough.<sup>18</sup> In contrast, our HPLC results demonstrated that a maximum of 11 h was needed to purify our sample of carbon dots. This purification duration, while considerable, is still shorter than the ~120 h cited by Beatrice Bartolomei and Maurizio Prato,<sup>18</sup> for C-dots synthesized through bottom-up techniques. Although top-down synthesis methods tend to yield a higher product volume, carbon dots produced *via* the

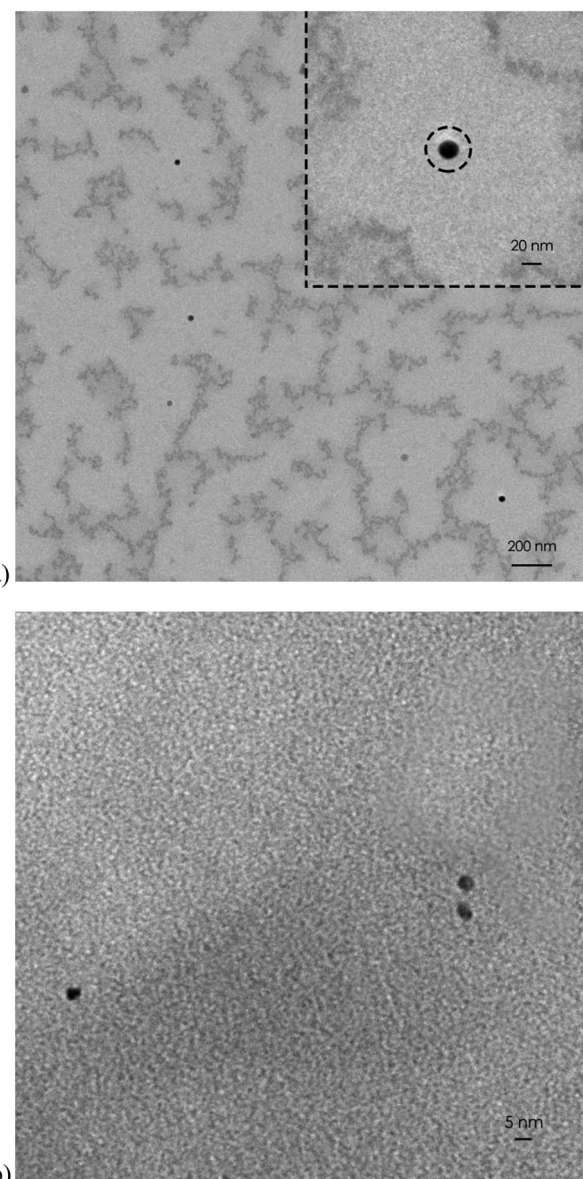


Fig. 2 TEM image of the C-dots (a) 20 nm (b) 5 nm.

bottom-up approach often possess superior purity.<sup>19</sup> Additionally, when carbon dots are derived using biomass, chiral or waste materials instead of refined chemicals, the synthesis might introduce a variety of contaminants. Consequently, deriving carbon dots from such biomass, chiral or waste materials remains a challenge due to these potential impurities, necessitating extended purification times.

The purified C-dots were further subjected to several different analysis. Transmission electron microscopy (TEM), FT-IR, X-ray photoelectron spectroscopy (XPS), and X-ray diffraction (XRD) results show that the core of C-dots is carbon, and the surface groups are functionalized by simple oxygen-related groups. The results confirm that C-dots have inherent visible emission spectra at 438 nm. This study provides a new way to prepare visible-emitting C-dots, which will greatly promote the application of C-dots (Fig. 2–5).

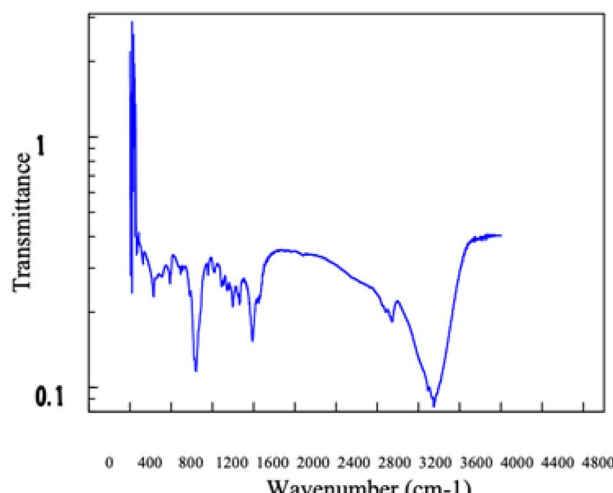


Fig. 3 FTIR spectrum of sample C-dots.

**3.1.1 TEM.** To gain insights into the shape and size of the prepared carbon dots, the samples was subjected to transmission electron microscopy (TEM) analysis. The resulting images revealed a uniform distribution of spheres with a consistent morphology, measuring between 5 and 20 nm in diameter (as seen in Fig. 2). The average diameter of the C-dots,

falling within this 5–20 nm range, aligns with typical measurements for synthesized C-dots.<sup>20</sup>

**3.1.2 FT-IR.** The functional groups present on the surface of C-dots significantly influence their properties. Indeed, the C-dots' optical attributes and solubility are intimately tied to these surface functional groups. The FTIR analysis was employed for characterization functional groups (Fig. 3). The broad peak between 3000 and 3600  $\text{cm}^{-1}$  is indicative of O-H and N-H functional groups. The moderate peak at 1600  $\text{cm}^{-1}$  suggests the stretching vibration of C=C bonds. Additionally, the faint absorption observed between 1200 and 1500  $\text{cm}^{-1}$  is likely associated with C-C bonds. The peak around 1100  $\text{cm}^{-1}$  could be corresponding to the presence of C-O, C-C, and C-N bonds. The FTIR analysis results suggest that a considerable amount of O-H, N-H, and C-N functional groups are present on the surface of the synthesized carbon dots. These groups also contribute to the high solubility of the C-dots.

**3.1.3 XPS.** To further study the impact of the C-dots' composition on their luminescent properties, we examine the high-resolution spectra featuring C 1s, N 1s, and O 1s peaks. In Fig. 4, the four characteristic peaks for the C 1s Gaussian fittings are located at 284.0, 285.0, 286.0, and 288.0 eV, which correspond to the  $\text{sp}^2$  hybridized C-dots-like carbon atoms, the  $\text{sp}^3$  hybridized carbon atoms, the O-C/3O groups, and the C-N/C-C-O groups, respectively. From the high-resolution spectra

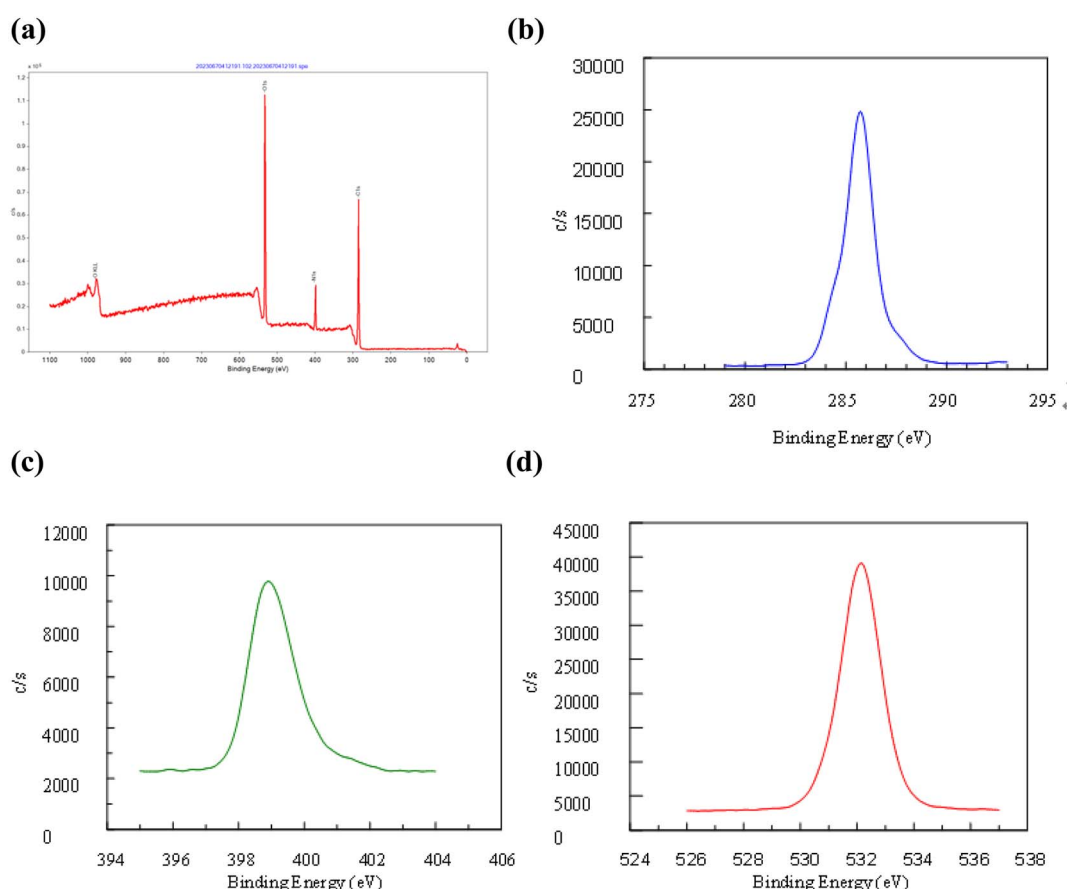


Fig. 4 XPS full spectrum (a), fine spectrum of C 1s (b), fine spectrum of N 1s (c), fine spectrum of O 1s (d) of C-dots.



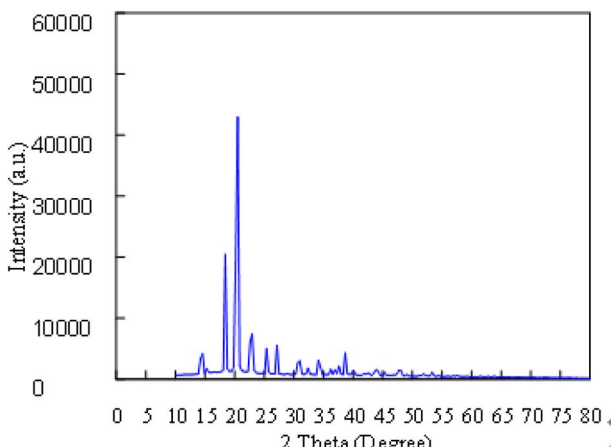


Fig. 5 XRD of the C-dots showing typical Bragg's reflections.

of N 1s, the binding energy peaks of the C-dots nitrogen are 398.5 and 400.5 eV, respectively. This indicates that the C-dots' surface was altered by Tris base groups, suggesting the Tris base's involvement in carbon nucleus formation during the synthesis. For O 1s, binding energies at 531.0, 532.2, and 533.1 eV are associated with the C–O and O–H bonds. Overall, the fitting peaks for C 1s, N 1s, and O 1s confirm that the synthesized C-dots comprise both  $sp^2$  and  $sp^3$  carbons. Additionally, their surfaces are enriched with nitrogen and –OH functional groups.

**3.1.4 XRD.** The X-ray diffraction pattern (XRD) depicted in Fig. 5 reveals the diffraction peaks of the C-dots synthesized *via* the hydrothermal method. These peaks emerge at  $2\theta = 19.0^\circ$ ,  $21.5^\circ$ , and  $23.0^\circ$ , which correspond to the (002)-diffraction peak of the C-dots. Notably, the C-dots exhibit prominent crystallinity. This can be attributed to the highly reactive nitrogen group in Tris base, which played a role in forming the carbon nucleus of the C-dots. This is because the internal structure of the C-dots' carbon nucleus is more ordered and stable, leading to enhanced crystallinity. The subdued intensity of this Bragg peak aligns with the diminutive size of the C-dots. Furthermore, Bragg peaks associated with L-lactose, which was used as the starting material, are absent.<sup>21–23</sup>

### 3.2 Formation of C-dots – impacts of carbon sources and surface passivation reagents

In current study, we utilized a “bottom-up” strategy to synthesize C-dots through a straightforward hydrothermal process. Three different carbon sources: lactose, glucose, and sucrose, were tested in conjunction with the Tris base for surface passivation. Successful C-dot synthesis was achieved using either lactose or glucose under our experimental conditions. Notably, although lactose and sucrose share an isomeric structure ( $C_{12}H_{22}O_{11}$ ), they yielded differing results. Lactose-derived C-dots possess strong fluorescence, while those from sucrose did not. This discrepancy can be attributed to the following two reasons:

(1) Lactose interacts with Tris to form a pyrrolic ring. In contrast, the planar tetrahydrofuran ring in sucrose prevents

pyrrolic ring formation. Additionally, the  $\alpha$ -1,4-glycosidic bond in sucrose challenges carbon core passivation as it positions the hydrogen atoms linked to C1 and C5 on opposite sides of the ring.

(2) Lactose contains an active hydroxyl group within its hemiacetal structure, a feature absent in sucrose. Under the gentle conditions of our study, this hydroxyl group might have significantly impacted carbon core formation by triggering

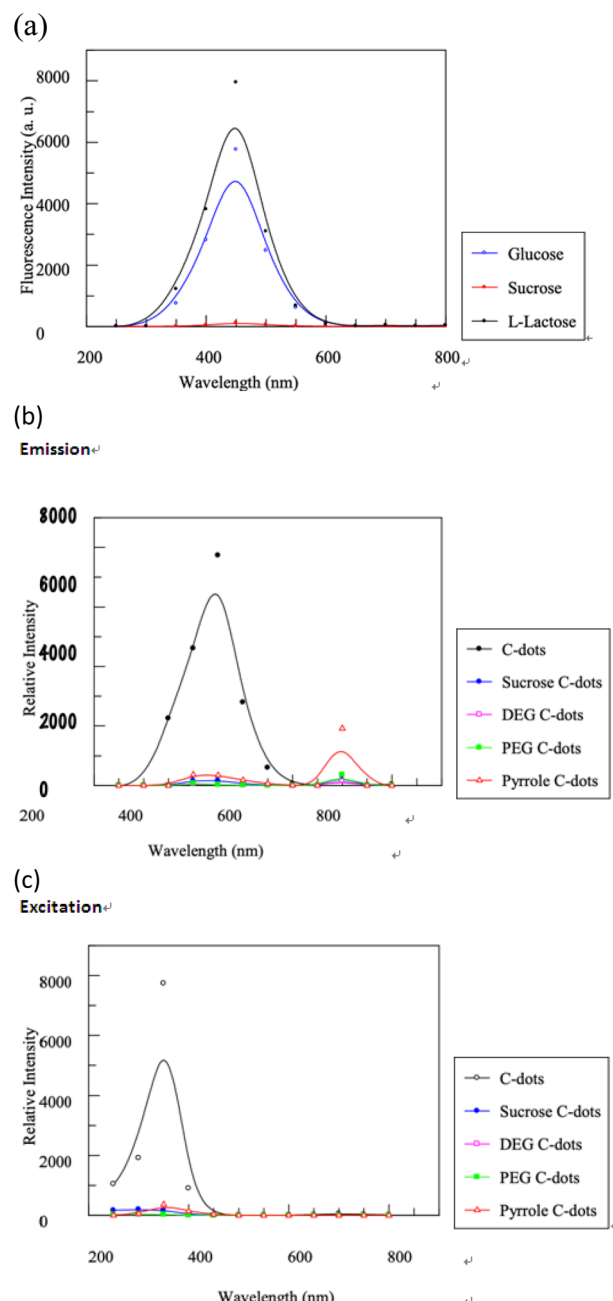


Fig. 6 Three types of carbon source: lactose (black), glucose (blue), and sucrose (red) and found that C-dots could be successfully synthesized using only lactose or glucose (a). Three small organic compounds as potential surface passivation agents: Tris base, diethylene glycol, and polyethylene glycol (PEG-200) were also examined fluorescence C-dots effective (b and c).



a condensation reaction between two saccharides before carbonization.

Additionally, as depicted in Fig. 6(a), substituting glucose with lactose led to a quantum yield surge in C-dots by roughly 45.3% (from 8.6% to 12.5%). This increase might stem from glucose's aqueous solution state. Unlike lactose's two relatively stable rings, glucose exists partly as a chain structure, which isn't ideal for carbonization and forming a consistent carbon core. Under basic conditions, glucose might transform into mannose and fructose *via* epimerization, as shown in Fig. 7.<sup>24</sup> These monosaccharides may not interact well with Tris base due to their structural properties, resulting in lower quantum yields in glucose-derived C-dots compared to those synthesized using lactose.

Three small organic compounds as potential surface passivation agents: Tris base, diethylene glycol, and polyethylene glycol (PEG-200) were also examined in the current study. Fluorescent C-dots were effectively created with Tris base (as shown in Fig. 6(b) and (c)). Yet, passivation with diethylene glycol or PEG-200 yielded no detectable luminescence. Analyzing the molecular structures of these agents, we believe that the presence of an amino group (or secondary amine) significantly impacts the synthesis. Hence, nitrogen, especially in the form of an amino group, appears to be pivotal for intense fluorescence emission. Tris likely amplified fluorescence for several reasons. Being an alkali, Tris sets up an alkaline environment conducive to carbon core formation. Moreover, its inherent amino group renders Tris an efficient surface passivation agent for C-dots (illustrated in Scheme 1). During the

process, the luminescent C-dot synthesis and surface modification might have transpired concurrently. Notably, in separate reflux experiments, neither lactose nor Tris displayed any photoluminescence. Furthermore, the chosen passivation agents influenced not only the fluorescence intensity but also the C-dots' emission wavelength. Specifically, Tris-passivated C-dots showcased blue fluorescence with a peak emission at 438 nm.

### 3.3 Stability of C-dots

A range of experiments were carried out to assess the stability of the synthesized C-dots, considering factors such as pH, salt concentration and UV exposure duration. Understanding these stability parameters is vital as the C-dots are intended for various practical uses, which might involve diverse salt concentrations and pH levels. In addition, for commercial applications, it's essential that the C-dots exhibit exceptional photostability.

**3.3.1 Effects of reflux duration and initial pH.** The fluorescence emission initially increased markedly as the reflux time increased and stabilized after 6 hours. However, the quantum yield of the C-dots declined after 28 hours, potentially due to their aggregation. The initial pH of the mixture played a pivotal role in the formation of the C-dots. Alkaline conditions were more conducive to the preparation process. Not only did pH influence the fluorescence intensity of the resulting C-dots, but it also triggered a blue shift in emission, with the peak wavelength transitioning from 490 nm to 440 nm. Fig. 8(a) illustrates that the optimum fluorescence intensity was achieved when the initial pH was set to 10.5. Owing to the

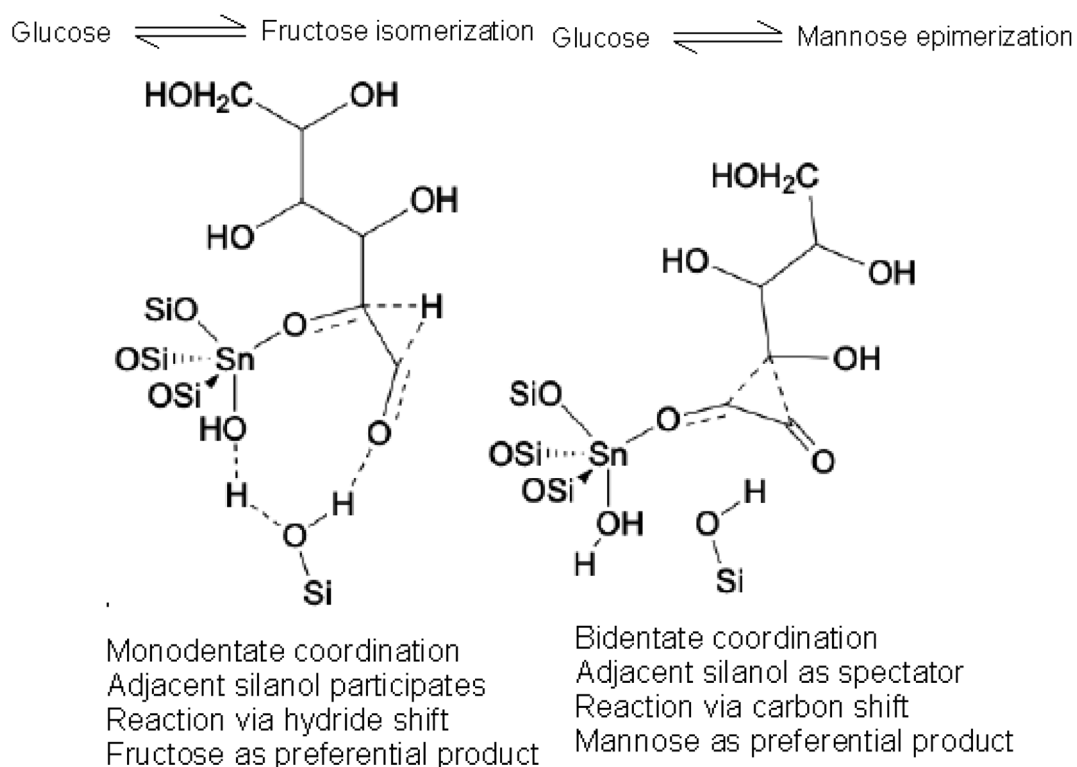
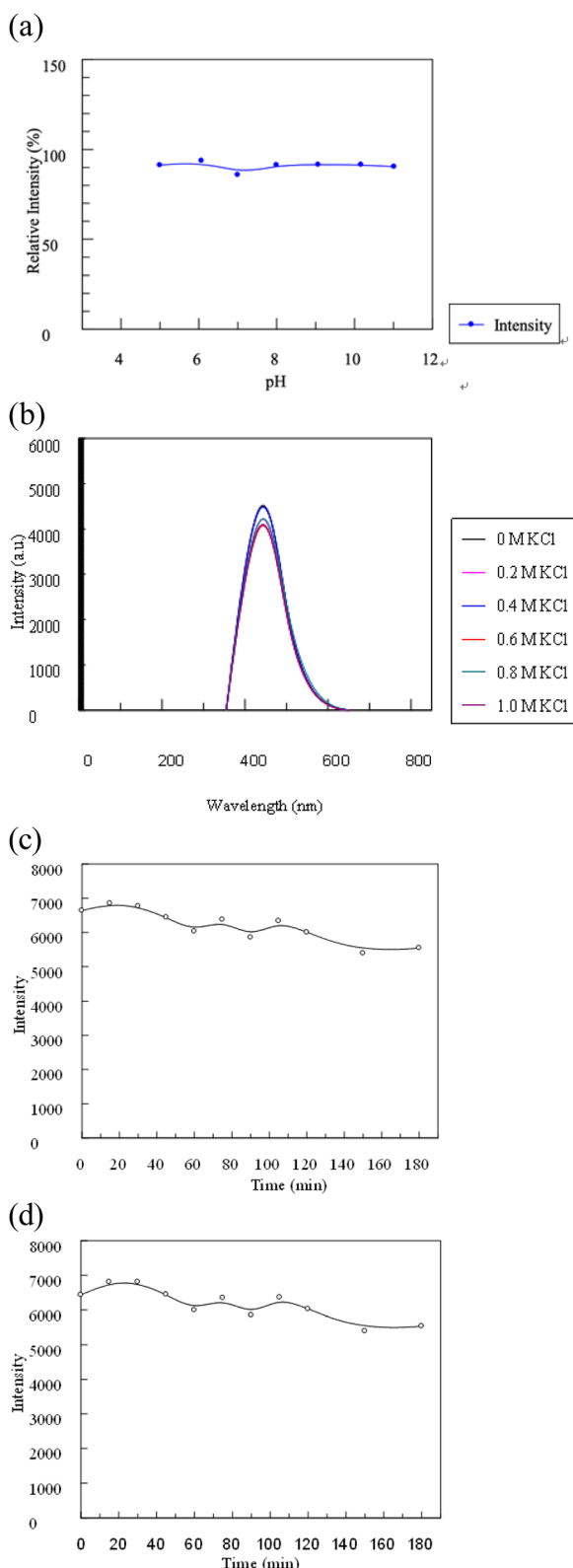


Fig. 7 Glucose is converted into mannose and fructose partly under the alkalescence condition through epimerization.





**Fig. 8** The influence of pH on the stability of C-dots (a). Ionic strength (b). A study on the effect of exposure time towards C-dots fluorescence characteristics is carried out where C-dots samples were stored under continuous UV radiation at 365 nm for 180 minutes. Emission spectrum of C-dots. (c). Excitation spectrum of C-dots. (d).

ionization of Tris, the mixture naturally stabilized at a pH of approximately 10.5, eliminating the need for additional pH adjusters.

**3.3.2 Ionic strength.** Fig. 8(b) showcases the impact of ionic strength on the photoluminescence (PL) intensity. Interestingly, elevating the KCl concentration had no significant effect on the fluorescence intensity of the C-dots. This suggests the resilience of the C-dots solution against salt disturbances. The consistent ionic strength of KCl appears to help prevent C-dots aggregation, as evidenced by the absence of precipitation even when 1.0 M of KCl was added. These observations highlight the robust KCl resistance of C-dots derived from *l*-lactose, making them suitable for biochemistry applications.

**3.3.3 Exposure duration.** The photostability of C-dots is critical for maintaining their optimal fluorescence attributes. To evaluate this, we assessed the fluorescence characteristics of C-dots under continuous UV radiation at 365 nm over a span of 180 minutes. Data from Fig. 8(c) and (d) reveals that, starting from the 15th minute up to the 180th minute, all samples consistently displayed peak absorption near the 438 nm wavelength. Furthermore, even after 180 minutes of exposure, the photoluminescence intensity remained steady at approximately 85%. This underscores the commendable photostability of the C-dots.

### 3.4 Selectivity and sensitivity of the C-dots

Seven common ions were employed in interference experiments to assess the selectivity and sensitivity of the C-dots. Fig. 9 illustrates the fluorescence intensities of C-dots when combined with different ions. To gauge the specificity and practicality of the synthesized C-dots for  $\text{H}_2\text{O}_2$  detection, we explored the fluorescence response of a variety of potentially interfering ions within the glucose/glucose oxidase/C-dots system at a set concentration, as depicted in Fig. 9. These investigations revealed that  $\text{H}_2\text{O}_2$  generated by the glucose/glucose oxidase enzymatic reaction can significantly reduce the fluorescence intensity of the C-dots in an aqueous solution in the presence of those tested ions. This enhanced selectivity for the enzyme reaction might be due to  $\text{H}_2\text{O}_2$ 's robust interaction with the C-dots compared to the other seven cations. As such, the C-dots/enzyme system offers promise as a “turn-off” fluorescence probe for  $\text{H}_2\text{O}_2$  detection. Fig. 10 displays the variations in fluorescence intensity of the C-dots throughout the proposed sensing process.

### 3.5 Optical properties of the C-dots

The key features of C-dots are their fluorescence properties, which were thoroughly examined using UV-visible and fluorescence spectroscopy. In a 0.2 mg  $\text{mL}^{-1}$  aqueous solution, the C-dots possessed two distinct UV-visible absorption peaks in the 270–310 nm range, as depicted in Fig. 11. These peaks likely arise from a combination of various electronic transitions.

Subsequently, a fluorescence map was derived by scanning the excitation wavelength from 280 to 500 nm for the enzyme reaction/C-dots and a blank solution, both set at pH 7.0. To



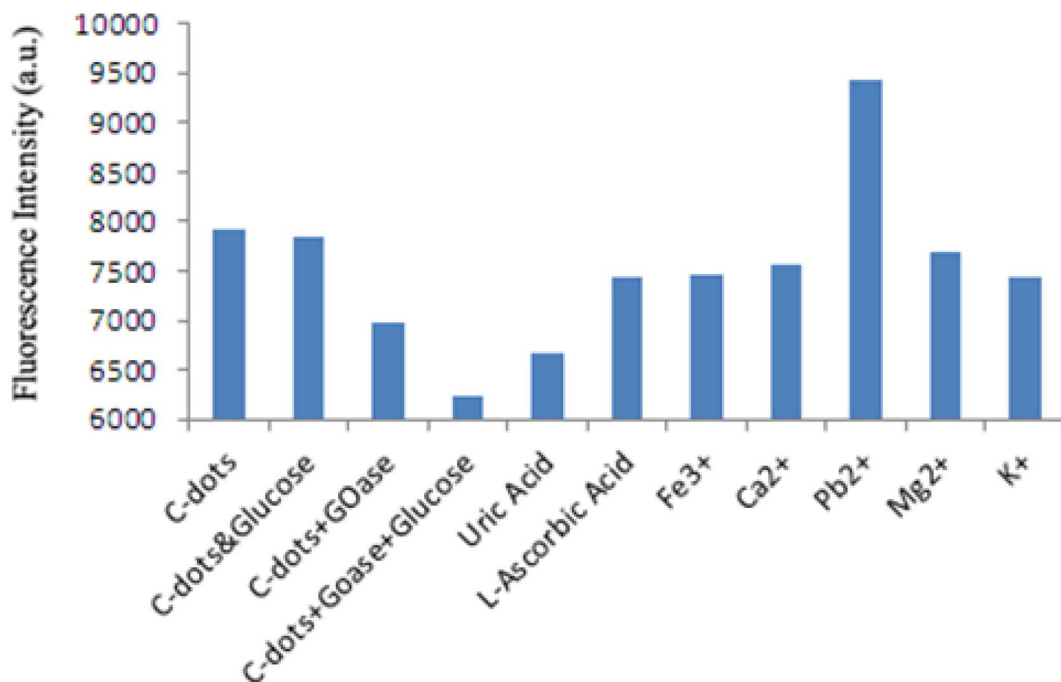


Fig. 9 Interference from other cation ion in the enzyme reaction/C-dots sensing solution.

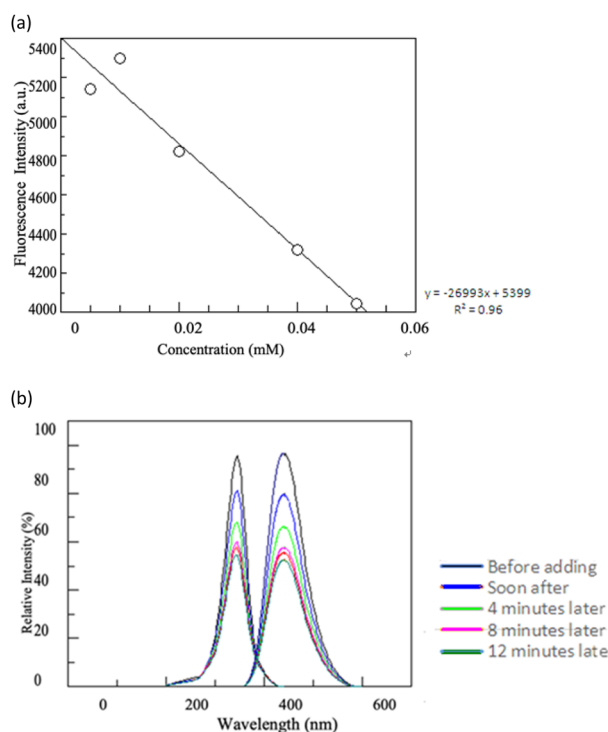


Fig. 10 Linear relationship between the fluorescence intensity ( $\lambda_{\text{em}} = 438 \text{ nm}$ ) and the glucose concentration. Glucose show linear behavior in 0.005–0.05 mM range (a). Fluorescence spectra of metabolite, biomolecule and carbon dots conjugate for different reaction durations (excitation wavelength, 348 nm; path length, 1 cm) (b).

ensure the fluorescence emanated specifically from the C-dots and wasn't influenced by the precursor, solvent, or secondary excitations, a control experiment using a lactose–water

solution (pH 7.0) was also conducted. The results revealed a pronounced fluorescence at 438 nm from the C-dots, suggesting their potential as robust fluorescent probes in the visible spectrum. To further confirm this finding, the fluorescence of varying concentrations of C-dots were assessed. It was observed that the intensity of the emitted fluorescence was directly proportional to the enzyme reaction/C-dots concentration, within the range of 25–3.125  $\mu\text{g mL}^{-1}$  (refer to Fig. 10(a) and (b)). The most intense fluorescence was detected at an excitation wavelength of 348 nm and an emission wavelength of 438 nm.

In our study, the fluorescence characteristics of C-dots produced through an aqueous hydrothermal method were assessed. As demonstrated in Fig. 12, the C-dots displayed characteristic absorption and photoluminescence patterns. There was a discernible absorption peak around 348 nm. Interestingly, these C-dots could be excited across a broad wavelength spectrum (285–385 nm). An emission peak of 380 to 470 nm can be detected when the C-dots were excited using wavelength ranges of 300 to 360 nm. The small full-width at half-maximum difference, approximately 90 nm, indicates a fairly consistent size distribution for these nanoparticles. Notably, the synthesized C-dots showcased both a pronounced Stokes shift and robust fluorescence.

Furthermore, the C-dots aqueous solution maintained stability for a remarkable six months; the fluorescence diminished only slightly by 4.8%, with no evidence of sedimentation, when stored at 4 °C. The quantum yield of these C-dots was gauged against quinine sulfate (used as a reference with an excitation wavelength of 410 nm).<sup>25</sup> Boasting a fluorescence quantum yield of 12.5%, these C-dots either matched or surpassed the yields of some previously documented C-dots.



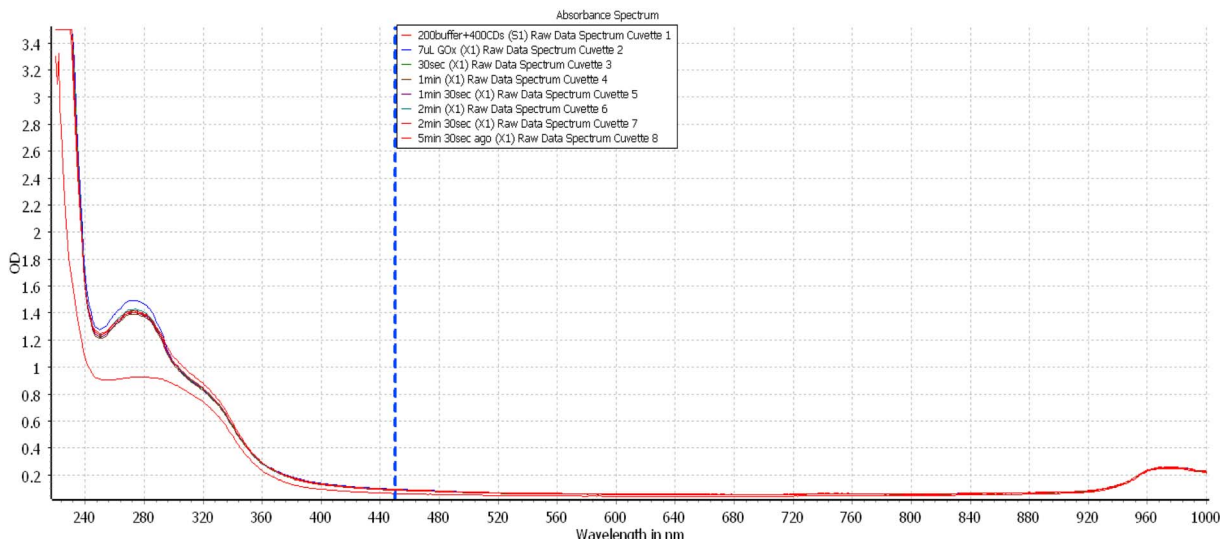


Fig. 11 Absorption spectra of the C-dots with enzyme reaction in difference time. Here, the concentration of enzyme and C-dots were the same in all cases.

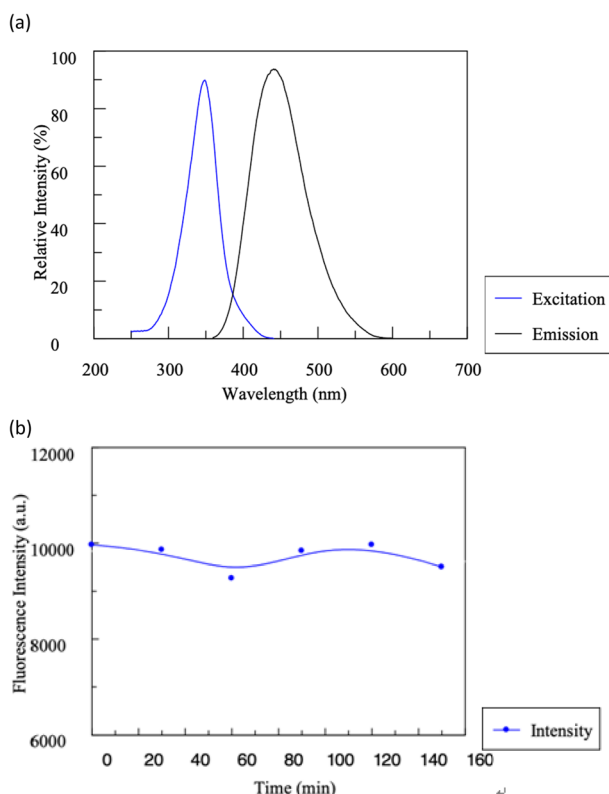


Fig. 12 Typical absorption and photoluminescence emission spectra of the C-dots (a). The influence of time on the stability of C-dots (b).

### 3.6 UV-vis spectra of the biocomposite and its enzymatic reactions

Fig. 11 presents the UV-vis absorption spectra of the biocomposite. Three peaks were observed at 270, 280, and 320 nm. The first two peaks were due to  $\pi-\pi^*$  transitions, and the third

was due to  $n-\pi^*$  transitions. The absorption peak of  $\beta$ -glucose oxidase was at 280 nm and that of the C-dots was at 320 nm. By adding glucose to the conjugate of  $\beta$ -glucose oxidase/C-dots biocomposite, the intensity of the absorption peaks quenched over time (Fig. 11).

### 3.7 Fluorescence spectra of the biocomposite

To further explore the formation of the biocomposite, we obtained the emission spectra of the biocomposite at excitation wavelengths ranging from 250 to 450 nm. The fluorescence spectra, shown in Fig. 10, depict the results of treating glucose with the biocomposite at the excitation wavelength of 348 nm. This particular wavelength was chosen due to its highest absorbance. Two primary bands emerged at 348 nm and 438 nm. The 348 nm absorption can be attributed to the aromatic amino acid residues from the associated enzyme, while the 438 nm emission is linked to the indigo component formed post-glucose oxidation. As evident from Fig. 10(b), the biocomposite facilitates glucose oxidation, indicated by the diminishing emission band at 438 nm over time. Typically, emission decreases as ROS levels rise, which is consistent with the hydrogen peroxide production from the enzyme coupling.

### 3.8 Fluorescence quenching of C-dots and glucose detection mechanism

In general, each C-dot has a surface passivation layer on its core to reduce the system's Gibbs free energy. When hydrophilic carbon precursors are used, hydrophilic C-dots are usually obtained, mainly because of the existence of rich hydroxyl, and amine groups on their surfaces. To modulate the properties of C-dots, modifiers such as Tris molecules are used to passivate their surfaces. When C-dots encounter ROS, such as singlet oxygen ( ${}^1\text{O}_2$ ), superoxide anion ( $\text{O}_2^-$ ), or hydroxyl radical ( $\cdot\text{OH}$ ), they can undergo quenching of their fluorescence *via* different



mechanisms. Here are a few possible quenching mechanisms involving ROS.<sup>26</sup>

(1) Electron transfer: C-dots can transfer electrons to ROS, leading to their reduction and subsequent quenching of the carbon dot fluorescence. The energy from the excited state of the carbon dot is used to reduce the ROS to a lower energy state, causing fluorescence quenching. Alternatively, C-dots can transfer their excited-state energy to ROS through a non-radiative energy transfer process. This energy transfer competes with the radiative decay process responsible for fluorescence emission, effectively reducing the fluorescence intensity.

(2) Oxidation of C-dots: certain ROS, such as singlet oxygen, can oxidize the C-dots' surface, resulting in the formation of various surface functional groups or defects. These modifications can alter the carbon dot's electronic structure, causing a decrease in fluorescence intensity.

(3) Reactive species-induced surface passivation: ROS can induce surface modifications on carbon dots that lead to the creation of non-emissive states or energy traps, which effectively quench the fluorescence.

Fig. 10 and 11 presents the detection mechanism of the proposed C-dot sensor. C-dots were covalently bonded with the enzyme, which led to a decrease in the fluorescence intensity (Fig. 10(b)). This reduction (50%) in the initial fluorescence of the C-dots indicated quenching in a turned-off system.

The aromatic residues in the enzyme and the -OH groups in the C-dots and glucose interact with the  $sp^2$  hybridization groups in the enzyme, bringing the enzyme closer to quench fluorescence. Glucose molecules interact with the enzyme due to their oxidation and the ability of the C-dots to irreversibly inhibit the enzyme. Consequently, the enzyme undergoes conformational changes,<sup>27</sup> leading to formation of the C-dot-enzyme complex. Thus,  $\pi$ -n interactions occur in the bio-composite, leading to fluorescence emission by the conjugate complex in the presence of glucose, is a highly distance-dependent fluorescence quenching ability.<sup>28</sup>

## 4. Conclusion

In this study, we showed that C-dots can be synthesized using L-lactose and Tris base by a hydrothermal method. The resulting C-dots can be further purified *via* a simple 11 hour dialysis procedure. Interestingly, these carbon dots demonstrated the feasibility of utilizing carbohydrates as a base. Yet, distinct differences in their PL properties emerged depending on whether the precursor was activated.

Fluorescent C-dots with strong blue emission at 438 nm have been innovatively designed and synthesized using a straightforward hydrothermal method. Remarkably, these C-dots have a quantum yield of 44.5%. Their exceptional stability across a pH range of 5–11 and resilience to various salt concentrations mark them as ideal candidates for biosystem sensing. Notably, their fluorescence intensity wanes in the presence of hydroxyl radicals, making them potent probes for fluorescence turn-off detection. By coupling these C-dots with glucose oxidase, glucose levels can be monitored in real-time. With their low

toxicity, these C-dots are poised to be invaluable in an array of detection techniques, especially when paired with the right substrates. We envision them playing a pivotal role in comprehensive metabolite monitoring in the future.

## Conflicts of interest

There are no conflicts to declare.

## Acknowledgements

We sincerely express our gratitude to the Ministry of Education of the Republic of China (Taiwan) for providing financial support and to Chung Shan Medical University for granting us access to essential instruments, significantly facilitating our research efforts. Our appreciation extends to the Instrumentation Center at National Tsing Hua University, with special thanks to Shang-Fang Chang, who offered valuable assistance with TEM techniques. Moreover, we are thankful to Ya-Hui Chen and the Precision Instrument Support Center at Feng Chia University for their expert support with XPS and XRD techniques. We also thank Chin-Hsuan Wan at the Institute of Visual Studies of National Yang Ming Chiao Tung University for helping with data analysis graph. The collective contributions of these individuals and institutions have played a vital role in the successful completion of our research project.

## References

- 1 X. Xu, R. Ray, Y. Gu, H. J. Ploehn, L. Gearheart, K. Raker and W. A. Scrivens\*, Electrophoretic Analysis and Purification of Fluorescent Single-Walled Carbon Nanotube Fragments, *J. Am. Chem. Soc.*, 2004, **126**, 12736.
- 2 V. G. Reshma and P. V. Mohanan, Quantum dots: Applications and safety consequences, *J. Lumin.*, 2019, **205**, 287.
- 3 W. A. A. Mohamed\*, H. A. El-Gawad, S. Mekkey, H. Galal, H. Handal, H. Mousa and A. Labib, Quantum dots synthetization and future prospect applications, *Nanotechnol. Rev.*, 2021, **10**, 1926.
- 4 A. AH Abdellatif, M. A. Younis, M. Alsharidah, O. Al Rugae and H. M Tawfeek, Biomedical Applications of Quantum Dots: Overview, Challenges, and Clinical Potential, *Int. J. Nanomed.*, 2022, **17**, 1951.
- 5 M. J. Molaei, Carbon quantum dots and their biomedical and therapeutic applications: a review, *RSC Adv.*, 2019, **9**, 6460.
- 6 B. Hasannejadasl, F. P. Janbaz, E. Choupani, M. Fadaie, M. A. Hamidinejad and D. Ahmadvand, *Thrita*, 2020, **9**(2), e100105.
- 7 J. Liu, R. Li and B. Yang\*, Carbon Dots: A New Type of Carbon-Based Nanomaterial with Wide Applications, *ACS Cent. Sci.*, 2020, **6**, 2179.
- 8 M. R. Biswal\* and S. Bhatia, Carbon Dot Nanoparticles: Exploring the Potential Use for Gene Delivery in Ophthalmic Diseases, *Nanomaterials*, 2021, **11**, 935.



9 V. S. Sivasankarapillai, A. V. Kirthi, M. Akksadha, S. Indu, U. D. Dharshini, J. Pushpamalar and L. Karthik, Recent advancements in the applications of carbon nanodots: exploring the rising star of nanotechnology, *Nanoscale Adv.*, 2020, 1760, DOI: [10.1039/C9NA00794F](https://doi.org/10.1039/C9NA00794F).

10 L. Cui, X. Ren, M. Sun, H. Liu and L. Xia, Carbon Dots: Synthesis, Properties and Applications, *Nanomaterials*, 2021, **11**, 3419, DOI: [10.3390/nano11123419](https://doi.org/10.3390/nano11123419).

11 F. Rigodanza, M. Burian, F. Arcudi and et al., Snapshots into carbon dots formation through a combined spectroscopic approach, *Nat. Commun.*, 2021, **12**, 2640, DOI: [10.1038/s41467-021-22902-w](https://doi.org/10.1038/s41467-021-22902-w).

12 R. Li, Z. Jia and M. A. Trush, Defining ROS in Biology and Medicine, *React. Oxygen Species*, 2016, **1**, 9, DOI: [10.20455/ros.2016.803](https://doi.org/10.20455/ros.2016.803).

13 B. C. dickinson and C. J Chang, Chemistry and biology of reactive oxygen species in signaling or stress responses, *Nat. Chem. Biol.*, 2011, **7**, 504, DOI: [10.1038/nchembio.607](https://doi.org/10.1038/nchembio.607).

14 S. J. Forrester, D. S. Kikuchi, M. S. Hernandes, Q. Xu and K. K. Griendling, Reactive Oxygen Species in Metabolic and Inflammatory Signaling, *Circ. Res.*, 2018, **122**, 877, DOI: [10.1161/CIRCRESAHA.117.311401](https://doi.org/10.1161/CIRCRESAHA.117.311401).

15 A. N. Vaneev, P. V. Gorelkin, A. S. Garanina, H. V. Lopatukhina, S. S. Vodopyanov, A. V. Alova, O. O. Ryabaya, R. A. Akasov, Y. Zhang, P. Novak, S. V. Salikhov, M. A. Abakumov, Y. Takahashi, C. R. W. Edwards, N. L. Klyachko, A. G. Majouga, Y. E. Korchev and A. S. Erofeev, *In Vitro* and *In Vivo* Electrochemical Measurement of Reactive Oxygen Species After Treatment with Anticancer Drugs, *Anal. Chem.*, 2020, **92**, 8010.

16 E. M. Espinoza, J. J. Røise, I.-C. Li, R. Das and N. Murthy, Advances in Imaging Reactive Oxygen Species, *J. Nucl. Med.*, 2021, **62**, 457, DOI: [10.2967/jnumed.120.245415](https://doi.org/10.2967/jnumed.120.245415).

17 G. C. V. d. Bittner, E. A. Dubikovskay, C. R. Bertozzia and C. J. Chang, *In vivo* imaging of hydrogen peroxide production in a murine tumor model with a chemoselective bioluminescent reporter, *Proc. Natl. Acad. Sci. U.S.A.*, 2010, **107**, 21316.

18 B. Bartolomei and M. Prato, The Importance of the Purification Step and the Characterization of the Products in the Synthesis of Carbon Nanodots, *Small*, 2023, **19**, 2206714.

19 R. B. González-González, L. T. González, M. Madou, C. Leyva-Porras, S. O. Martinez-Chapa and A. Mendoza, Synthesis, Purification, and Characterization of Carbon Dots from Non-Activated and Activated Pyrolytic Carbon Black, *Nanomaterials*, 2022, **12**, 298, DOI: [10.3390/nano12030298](https://doi.org/10.3390/nano12030298).

20 S. Dua, P. Kumar, B. Pani, A. Kaur, M. Khannaf and G. Bhatt, Stability of carbon quantum dots: a critical review, *RSC Adv.*, 2023, **13**, 13845–13861.

21 R. Lehmacher and C. Feldmann, Polyol-Mediated Synthesis of Nitrogen-Containing Carbon-Dots from Tetracyanobenzene with Intense Red Fluorescence, *Nanomaterials*, 2019, **9**, 1470, DOI: [10.3390/nano9101470](https://doi.org/10.3390/nano9101470).

22 V. Arul and M. G. Sethuraman, Hydrothermally Green Synthesized Nitrogen-Doped Carbon Dots from *Phyllanthus emblica* and Their Catalytic Ability in the Detoxification of Textile Effluents, *ACS Omega*, 2019, **4**, 3449–3457, DOI: [10.1021/acsomega.8b03674](https://doi.org/10.1021/acsomega.8b03674).

23 Y. Bian, B. He and J. Li, A One-step Hydrothermal Method of Nitrogen-doped Graphene Quantum Dots Decorated Graphene for Fabrication of Paper-based Fluorescent Composite, *BioResources*, 2016, **11**(3), 6299–6308.

24 I. Delidovich and R. Palkovits, Catalytic Isomerization of Biomass-Derived Aldoses: A Review, *ChemSusChem*, 2016, **9**, 547, <https://www.chemsuschem.org>.

25 I. Alkian, H. Sutanto and H. Hadiyanto, Quantum yield optimization of carbon dots using response surface methodology and its application as control of  $Fe^{3+}$  ion levels in drinking water, *Mater. Res. Express*, 2022, **9**, 015702.

26 F. Noun, E. A. Jury and R. Naccache, Elucidating the Quenching Mechanism in Carbon Dot-Metal Interactions—Designing Sensitive and Selective Optical Probes, *Sensors*, 2021, **21**, 1391, DOI: [10.3390/s21041391](https://doi.org/10.3390/s21041391).

27 M. Li, X. Zhou, S. Guo and N. Wu, Detection of lead (II) with a “turn-on” fluorescent biosensor based on energy transfer from CdSe/ZnS quantum dots to graphene oxide, *Biosens. Bioelectron.*, 2013, **43**, 69.

28 P. Reineck, D. Gómez, S. H. Ng, M. Karg, T. Bell, P. Mulvaney and U. Bach, Distance and Wavelength Dependent Quenching of Molecular Fluorescence by  $Au@SiO_2$  Core-Shell Nanoparticles, *ACS Nano*, 2013, **7**, 6636, DOI: [10.1021/nn401775e](https://doi.org/10.1021/nn401775e).

